The respective role of atmospheric carbon dioxide and orbital parameters on ice sheet evolution at the Eocene-Oligocene transition

Jean-Baptiste Ladant, Yannick Donnadieu, Vincent Lefebvre, Christophe Dumas

AGU PUBLICATIONS

Paleoceanography

RESEARCH ARTICLE
10.1002/2013PA002593

Key Points:
- Transient simulations of the ice evolution at the Eocene-Oligocene transition (34–33.5 Myr)
- Good agreement between results and data revealing a two-stepped transition
- Simulations explore the impact of CO_2 and orbital parameters on the ice sheet

Correspondence to:
J.-B. Ladant,
jean-baptiste.ladant@lsce.ipsl.fr

Citation:
Ladant, J.-B., Y. Donnadieu, V. Lefebvre, and C. Dumas (2014), The respective role of atmospheric carbon dioxide and orbital parameters on ice sheet evolution at the Eocene-Oligocene transition, *Paleoceanography*, *29*, 810–823, doi:10.1002/2013PA002593.

Received 4 DEC 2013
Accepted 6 AUG 2014
Accepted article online 11 AUG 2014
Published online 25 AUG 2014

The respective role of atmospheric carbon dioxide and orbital parameters on ice sheet evolution at the Eocene-Oligocene transition

Jean-Baptiste Ladant[1], Yannick Donnadieu[1], Vincent Lefebvre[1], and Christophe Dumas[1]

[1]Laboratoire des Sciences du Climat et de l'Environnement, CEA-CNRS-UVSQ, Gif-sur-Yvette, France

Abstract The continental scale initiation of the Antarctic ice sheet at the Eocene-Oligocene boundary (Eocene-Oligocene transition (EOT), 34 Ma) is associated with a global reorganization of the climate. If data studies have assessed the precise timing and magnitudes of the ice steps, modeling studies have been unable to reproduce a transient ice evolution during the Eocene-Oligocene transition in agreement with the data. Here we simulate this transition using general circulation models coupled to an ice sheet model. Our simulations reveal a threshold for continental scale glaciation of 900 ppm, 100 to 150 ppm higher than previous studies. This result supports the existence of ephemeral ice sheets during the middle Eocene, as similar CO_2 levels (900–1000 ppm) have been reached episodically during this period. Transient runs show that the ice growth is accurately timed with EOT-1 and Oi-1, the two $\delta^{18}O$ excursions occurring during the transition. We show that CO_2 and orbital variations are crucial in initiating these steps, with EOT-1 corresponding to the occurrence of low summer insolation, whereas Oi-1 is controlled by a major CO_2 drop. The two $\delta^{18}O$ steps record both ice growth and temperature, representing some 10–30 m eustatic sea level fall and 2–4°C cooling at EOT-1 and 70 ± 20 m and 0–2°C for Oi-1. The simulated magnitude of the ice steps (10 m for EOT-1 and 63 m for Oi-1) and the overall cooling at various locations show a good agreement with the data, which supports our results concerning this critical transition.

1. Introduction

At the Eocene-Oligocene transition (34–33.5 Ma), a continental scale ice sheet started to develop over Antarctica with climatic consequences at a global scale. It has been suggested that ephemeral (1 Myr) ice sheets might have already been present over Antarctica during the middle Eocene [*Browning et al.*, 1996; *Dawber and Tripati*, 2011; *Miller et al.*, 2005; *Pekar et al.*, 2005; *Tripati et al.*, 2005], but this issue still lacks strong evidence and is therefore widely debated. Conversely, several bodies of evidence arising from oxygen isotope excursions, temperature reconstructions, and stratigraphic records support a continental scale ice growth occurring at the Eocene-Oligocene transition (EOT). Benthic foraminiferal $\delta^{18}O$ records show an overall 1.5‰ two-step increase during the EOT [*Bohaty et al.*, 2012; *Zachos et al.*, 2001]. This evolution has been widely recorded in sediments from many different locations [*Coxall et al.*, 2005; *Katz et al.*, 2008; *Lear et al.*, 2008; *Pusz et al.*, 2011; *Scher et al.*, 2011] as well as in sea level reconstructions showing large-amplitude falls [*Houben et al.*, 2012; *Katz et al.*, 2008; *Miller et al.*, 2009]. These data studies hence demonstrated that the first $\delta^{18}O$ step ("EOT-1" or the "precursor" event) is due to a global cooling with a modest ice growth component, whereas the second step ("Oi-1") mainly represents the major ice growth leading to a continental scale ice sheet over Antarctica [*Miller et al.*, 2009].

The reasons for this greenhouse-icehouse transition have long been debated, mainly between the "tectonic-oceanic" hypothesis and the CO_2 hypothesis. The first one states that the opening of the southern passages (the Drake and Tasman seaways) has permitted the development of the Antarctic Circumpolar Current (ACC), hence isolating Antarctica from warmer tropical transport of waters [*Kennett*, 1977; *Kennett and Exon*, 2004]. As a result, the cooling due to oceanographic changes would have enabled the growth of considerable ice volume. The second hypothesis suggests that the crucial factor in the late Eocene ice expansion is the atmospheric CO_2 partial pressure drawdown. It is supported by independent proxies showing a fall of pCO_2 from concentrations largely above 1000 ppm during the Eocene to levels below 800 ppm at the EOT [*Beerling and Royer*, 2011; *Pagani et al.*, 2005; *Pagani et al.*, 2011; *Pearson et al.*, 2009]. Modeling studies also support a first-order control of the pCO_2 compared to the effects of the tectonic-oceanic reorganization.

DeConto and Pollard [2003b] have shown that the decrease in atmospheric CO_2·levels occurring at the Eocene-Oligocene boundary has a far larger effect on the growth of the Antarctic ice sheet than the potential change in oceanic heat transport arising from the opening of the Drake Passage. More recently, *Lefebvre et al*. [2012] have shown that for pCO_2 typical of the EOT, only a very weak ACC develops, suggesting that the ACC was a consequence, having a positive feedback on the cooling of Antarctica, rather than the main cause of the initiation of large-scale ice sheets.

While the primary effect of the atmospheric CO_2 has been emphasized several times these previous years, few numerical simulations have focused on the accurate timing of the Antarctica ice sheet build up. *Tigchelaar et al*. [2011] used a box model to reproduce the two-step $\delta^{18}O$ signal when forced by a decreasing atmospheric CO_2 concentration. They found that the first step represents a deep-sea cooling recording a meridional overturning circulation shift, while the second step embodies rapid and massive Antarctic glaciation. However, the change in meridional overturning circulation invoked in their analysis leads to an increase in ice volume occurring in only one step, whereas the data indicate a two-step ice growth, with a modest ice component contributing to the first excursion (EOT-1) in $\delta^{18}O$ records [*Houben et al*., 2012]. Previously, *Pollard and DeConto* [2005] ran 10 Myr simulations across the EOT to investigate the hysteresis induced by the Antarctic ice sheet buildup and decay. When decreasing the CO_2 across the transition, their model simulates a two-step increase in ice volume; the shape of which is very similar to proxy records. Nevertheless, the timing (and amplitude) of the transition was not the main focus of their paper. Indeed, they used idealized orbital variations, which prevented them from going into further details concerning the exact timing of the transition. In addition, the way they accounted for ice sheet feedback deserves improvements, as they did not take into account the ice-albedo feedback on long-term runs.

Here we use a set of asynchronously coupled models to bring new insights on the initiation of the Antarctic ice sheet following a method whose framework has been suggested by *Pollard* [2010] and which is based on the original works of *DeConto and Pollard* [2003a, 2003b] and *Pollard and DeConto* [2005]. One of the main improvements from these studies lies in the use of the astronomically reconstructed insolation of *Laskar et al*. [2004] instead of using idealized orbital parameter variations corresponding to idealized sinusoidal periods of 20, 40, and 80 kyr for precession, obliquity, and eccentricity variations, respectively [*DeConto and Pollard*, 2003a; *Horton and Poulsen*, 2009]. The method consists in running an ice sheet model with interpolated forcings derived from equilibrated climatic snapshots representing different climatic states over Antarctica. By taking into account both the height-mass balance and the ice-albedo feedback, our results suggest that the CO_2 threshold that enable the initiation of large-scale glaciation is 100–150 ppm higher than what was previously thought [*DeConto and Pollard*, 2003a]. This higher value provides support to the possible existence of substantial ice sheets throughout the Eocene [*Miller et al*., 2005] and remains close to the upper bound of the threshold range derived from the intermodel comparison of *Gasson et al*. [2014]. We develop a method of interpolation enabling us to reproduce the shape of the Eocene-Oligocene transition. Our results display a timing of the steps at 33.9 and 33.7 Myr very well correlated with astronomically dated oxygen isotopes records. Besides, the magnitude of these two steps is in agreement with a first modest ice increase during EOT-1 (10 to 25 m of equivalent sea level) and a second major growth during Oi-1 (50 to 80 m). In addition, the simulated ocean temperature cooling of 1.5 to 4°C produced by our model is also consistent with reconstructed oceanic cooling recorded at both low- and high-latitudes sites.

2. Models and Methods

2.1. Models

It is currently infeasible to use a general circulation model (GCM) fully coupled to an ice sheet model (ISM) owing to the time that would be needed to simulate hundreds of thousands of years. The only way to simulate ice sheet variations on long time scales (few tens of kiloyears or more) involves asynchronous coupling between a GCM and an ISM. A review of these techniques has been extensively presented by *Pollard* [2010]. The most straightforward is the asynchronous method that consists of running the ISM continuously while updating the climate forcing by running the GCM approximately every thousand years with the updated ice sheet configuration and the updated current state of other time-variable parameters. *Herrington and Poulsen* [2011] have recently applied this method to the expansion of the Laurentide ice sheet

after the last interglacial and have shown the importance of the time interval between two GCM updates. As our purpose is to simulate the whole Eocene-Oligocene transition, which lasts several hundreds of thousands of years, the limitations in computing time prevent us from using this method. Instead, we have used a matrix method in which several climatic snapshots, spanning a range of possibilities for the ice sheet area, the CO_2, and the orbital variations, are gathered to create an interpolated climatic forcing to drive the ISM [*Pollard*, 2010]. Preliminary versions of this method have already been applied to the Eocene-Oligocene transition in Antarctica [*DeConto and Pollard*, 2003a, 2003b; *Pollard and DeConto*, 2005]. A more sophisticated version refining these pioneering studies is developed here.

Here we set up a 3-D matrix, which contains several climatic snapshots varying according to three metrics: the Earth's orbital parameters, the ice sheet area, and the atmospheric pCO_2. The climatic fields will be interpolated according to time variations of (1) the insolation over Antarctica, (2) the ice sheet area, and (3) the atmospheric CO_2 levels. In this study, the oceanic cooling produced by our model at the EOT is used for a data-model comparison exercise. This requires the use of a coupled ocean-atmosphere model to simulate the temperature of the deep ocean. The coupled ocean-atmosphere model has to be very efficient in terms of computational time, given the number of climatic snapshots we need to build our 3-D matrix. These snapshots are hence created using the fully coupled mixed-resolution atmosphere-ocean GCM FOAM (Fast Ocean Atmosphere Model). The atmospheric component of FOAM is the Parallel Community Climate Model version 3–University of Wisconsin, which is mainly constituted of the parallel version of NCAR's Community Climate Model, version 2 (CCM2) model with modified physics routines so that the atmospheric physics is equivalent to the CCM3 model. The atmospheric component has 18 vertical levels with the R15 spectral resolution (7.5° in longitude × 4.5° in latitude). The ocean component is the Ocean Model version 3, a finite difference, *z* coordinate model that is dynamically similar to the GFDL Modular Ocean Model (MOM) and is optimized for distributed memory-parallel platforms [*Jacob*, 1997]. It has 24 vertical levels, with 12 in the upper 1000 m, and a 128 × 128 resolution (2.8° × 1.4°) on a regular polar grid. The sea ice model uses the thermodynamics of NCAR's CSM Sea Ice Model version 2.2.6. It is implemented together with the CCM2 land model by the coupler that links the ocean and the atmospheric components. The FOAM model has been thoroughly used to simulate past climates [*Donnadieu et al*., 2009; *Lefebvre et al*., 2012; *Poulsen and Jacob*, 2004].

Since the coarse resolution of the atmospheric component of FOAM does not enable the direct use of the temperature and precipitation fields as inputs for our ice sheet model GRISLI (GRenoble Ice Shelves and Land Ice model), the GCM-ISM coupling is achieved in two steps. We couple FOAM with the LMDZ (Laboratoire de Météorologie Dynamique Zoom) model by forcing LMDZ with sea surface temperature (SST) averaged over the last 100 years of equilibrated FOAM simulations, all other boundary conditions being kept identical. Temperature and precipitation fields averaged on the last 5 years of equilibrated 20 yearlong LMDZ simulations are then stored in our climatic matrix in order to force the GRISLI ISM. LMDZ constitutes the atmospheric component of the IPSL (Institut Pierre-Simon Laplace) coupled model. It uses a longitude-latitude-staggered Arakawa C-grid to discretize the dynamical equations and ensure the conservation of both enstrophy and angular momentum [*Hourdin et al*., 2006]. The version we use here has 39 vertical levels and runs on a 96 × 95 resolution (3.75° × 1.9°). GRISLI is a time-dependent 3-D ice sheet model, accounting for thermomechanical coupling between flow and temperature, that has been developed and validated over Antarctica by *Ritz et al*. [2001]. The model runs at 40 km × 40 km resolution and simulates the dynamics of grounded and floating ice but also ice shelves and ice stream regions. GRISLI also models the depression and rebound of bedrock elevations with a time constant of 3 kyr.

2.2. Method Description and Boundary Conditions

The climatic snapshots are created by running FOAM to equilibrium for 2000 years with the early Oligocene paleogeography used by *Lefebvre et al*. [2012] at the exception of the reconstructed Antarctic topography. The paleogeography follows *Scotese* [2001] with subsequent changes in the Tethys [*Barrier and Vrielynck*, 2008] and central American [*Iturralde-Vinent and MacPhee*, 1999] seaways, while the paleobathymetry is established following *Bice et al*. [1998]. In this reconstructed geography, the Drake and Tasman gateways are open. Australia is closer to Antarctica than in present-day configuration, while South America is very close to its modern position. The Panama seaway is open, and the Tethys connects the Indian and Atlantic oceans; the latter being more constricted than today (Figure 1). The Antarctic topographic reconstruction

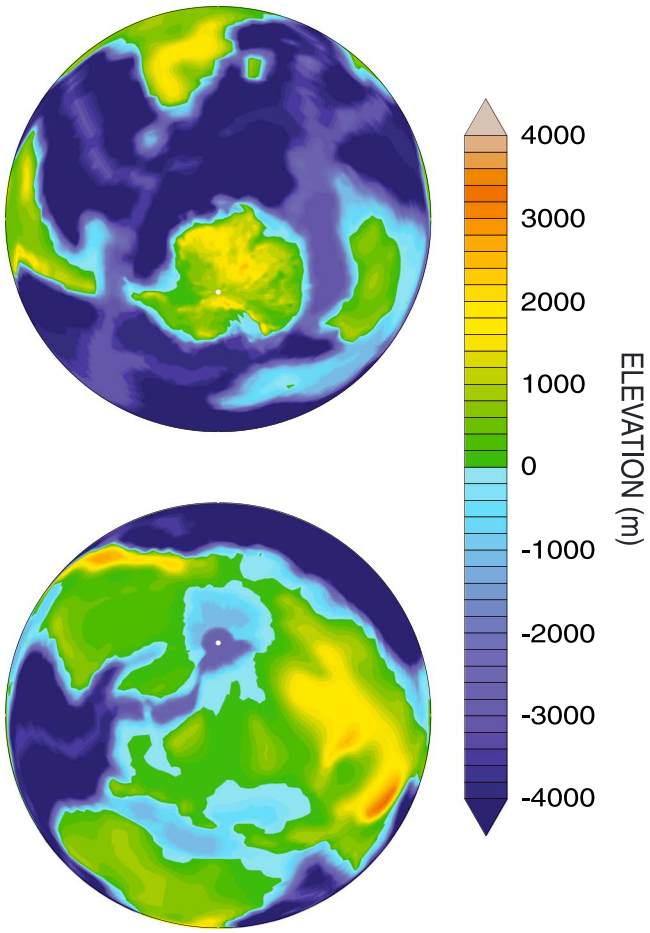

Figure 1. Early Oligocene paleogeography.

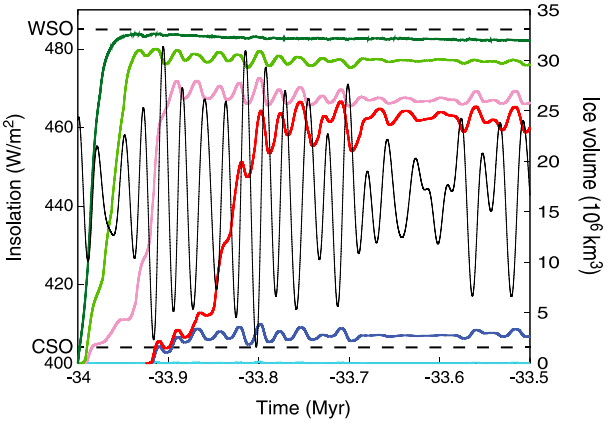

Figure 2. Antarctic ice sheet evolution at the EOT for different pCO_2. The colored curves represent the evolution of the ice volume versus time with CO_2 levels of 980 ppm (cyan), 925 ppm (blue), 900 ppm (red), 840 ppm (violet), 700 ppm (green), and 560 ppm (dark green). The black curve is the variation of the austral summer (December-January-February) insolation at 65°S (available at http://www.imcce.fr/Equipes/ASD/insola/earth/earth.html). The dashed black lines represent the summer insolation at 65°S produced by the warm and cold summer orbit.

is taken from the larger estimate of *Wilson et al*. [2012]. This reconstruction does account for the history of the erosion over Antarctica and results in a larger land area than the isostatically adjusted ice-free present Antarctic topography used in most previous modeling studies [e.g., *DeConto and Pollard*, 2003a, 2003b], with the notable exceptions of *Wilson et al*. [2013] and *Stocchi et al*. [2013]. Other boundary conditions that differ from modern day include the atmospheric CO_2 levels, the orbital parameters, and the solar constant; the latter one being reduced to 1361 W m^{-2}. In this study, we use the atmospheric CO_2 levels ranging from 2 × PAL (preindustrial atmospheric levels, 280 ppm) to 4 × PAL: 560, 700, 840, 980, and 1120 ppm. With the assumption that Antarctic summer temperature is the crucial factor on the sustainability of ice sheets [*DeConto and Pollard*, 2003a], we use two opposed orbital configurations. These configurations either produce a warm summer orbit (WSO; eccentricity = 0.05, obliquity = 24.5°, and perihelion in January [*DeConto et al*., 2007]) or a cold summer orbit (CSO; eccentricity = 0.05, obliquity = 24.5°, and perihelion in July) over Antarctica. We then compute the mean summer insolation at 65°S between 34 and 33.5 Myr from the astronomical reconstructions of *Laskar et al*. [2004] (Figure 2, in black). For the sake of simplicity, we assume a linear relationship between climate and orbital parameters.

For each CO_2 concentration, we prescribe three ice sheet sizes derived from preliminary runs (Table 1) except at 1120 ppm, where the climate over Antarctica is too warm to enable the growth of an ice sheet, even in the CSO case. With the temperature and precipitation fields from the GCM results, we build a climatic matrix consisting of 2 (orbits) × 4 (three ice sheet sizes + ice free Antarctica) × 5 (CO_2) climatologies. At each ISM time step (1 year), we interpolate the most appropriate climatologies to force the

Table 1. Approximated Ice Volume of the Prescribed Ice Sheets Used to Build our Matrix

CO_2 (ppm)	Approximated Ice Volume (10^6 km^3)
560	10
	20
	33
700	8
	18
	28
840	6
	13
	24
980	3
	7
	11

ISM according to the current value of orbital parameters, ice sheet area, and CO_2 concentration. The whole triple interpolation calculation is done in three steps. First, a linear interpolation is realized according to the variations of the mean summer insolation at 65°S computed from the astronomical calculations (Figure 2). Second, a nonlinear interpolation (see below) is realized according to the ice sheet area. Third, a logarithmic interpolation is done according to the CO_2 variations. This method enables us to iteratively take into account, at each time step, not only the height mass balance feedback but also the strong ice-albedo feedback. In this study, the lapse rate correction is set at 5°C/km.

The interpolation with the ice sheet area metric is done following a new method that we have specifically developed. Indeed, classical linear interpolation may create artificially cold areas, favoring a very rapid ice growth and therefore possibly biasing the ice evolution. For instance, let us consider the linear interpolation between two ice sheet sizes of areas S_0 and S_1 (with $S_1 > S_0$) and climate forcings C_0 and C_1, the ice sheet area being S_0 at the start of the interpolation. Once additional ice starts to accumulate, the current ice sheet area S is only slightly larger than S_0, yet the climate forcing, determined by the linear interpolation relationship $C = R \times C_1 + (1 - R) \times C_0$ with $R = (S - S_0)/(S_1 - S_0)$, will impose interpolated conditions on the area corresponding to the S_1 ice sheet area, although the current size of the ice sheet is close to S_0, leading to a physically unrealistic behavior: the growth of a low relief but very spread ice sheet within a very short time, with ice nucleating on areas whose initial mass balance is negative. To illustrate this feature, we have run a 100 year ISM simulation with orbital parameters, and CO_2 kept constant starting with an ice-free Antarctica and evolving toward a prescribed ice sheet. Figure 3 (left) shows the initial mass balance over a $2.5 \times$ PAL CO_2 ice-free Antarctica under CSO orbital conditions. Positive mass balance is restricted to high reliefs (Gamburtsev and Transantarctic Mountains and Dronning Maud Land), yet after 100 years of simulation, ice has nucleated on almost the whole continent, and the ice sheet is already of continental size, which is unrealistic on such short time scale (Figure 3, middle).

The nonlinear method we have elaborated to address this issue aims at representing the progressive ice sheet buildup under the assumption that a newly glaciated continental grid point will only affect climate locally. The idea is to calculate an interpolated climate forcing for each Antarctic grid point instead of basically interpolating the whole grid between the two surrounding snapshots (of areas S_0 and S_1, as before with $S_1 > S_0$, and climates C_0 and C_1). For each grid point, the climate forcing is calculated by evaluating, within a

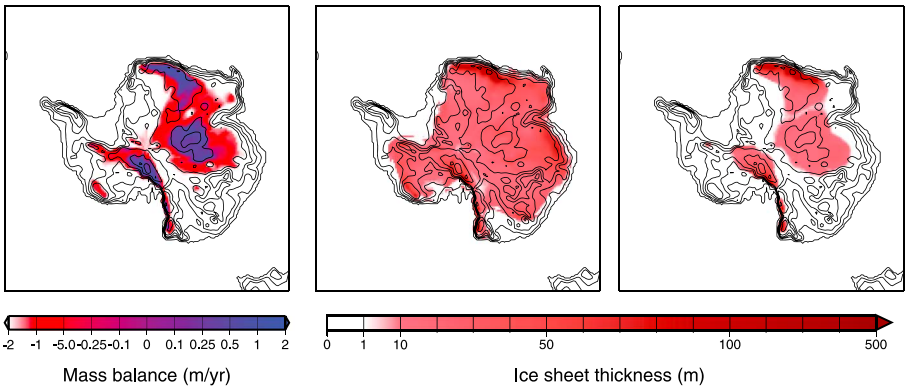

Figure 3. Comparison of the ice evolution for the linear and nonlinear methods of interpolation after 100 years of simulation. (left) Initial mass balance (ice free, $2.5 \times$ PAL CO_2, CSO conditions run). (middle) Ice thickness after 100 years for a linear interpolation. (right) The nonlinear method is shown.

Table 2. Maximum Ice Sheet Volume for Each pCO_2

CO_2 (ppm)	Approximated Maximum Ice Volume (10^6 km^3)	Maximum Ice State
560	32.5	Fully glaciated
700	31	Fully glaciated[a]
840	28	Largely glaciated[b]
900	26	Largely glaciated[c]
925	4	Three small ice sheets[d]
980	0.1	Two glaciers[e]
1120	0	Not applicable

[a]Except a small part of West Antarctica.
[b]Except the majority of West Antarctica and Victoria Land.
[c]Except West Antarctica and Victoria Land.
[d]Located on the Gamburtsev Mountains, the Transantarctic Mountains, and the Dronning Maud Land.
[e]Located on the Gamburtsev and Transantarctic Mountains.

certain radius, the proximity of the surrounding ice points with the grid point under scrutiny. Three possibilities might occur.

1. Within the radius, every point is glaciated. The ISM then uses the climate forcing of snapshot S_1.
2. Within the radius, every point is ice free. The ISM then uses the climate forcing of snapshot S_0.
3. Within the radius, there are both glaciated and ice-free points. A coefficient k representing the proximity of the number of glaciated points is calculated by giving a larger weight to grid points close to the focused point. This coefficient is then used to linearly interpolate the climate between snapshots S_0 and S_1:

$$C = k \times C_1 + (1 - k) \times C_0.$$

Repeating the previous experiment with the same initial and boundary conditions, we observe that after 100 years, ice has accumulated on a smaller area that is almost restricted to positive mass balance areas (Figure 3, right), and ice growth follows a step-by-step circular expansion, which seems more correct regarding the dynamical behavior of the ice. However, we want to underline that this new interpolation method, although physically more realistic than a simple linear interpolation, is not an attempt to accurately model the physics of the ice or its behavior and remains an ad hoc parameterization of climate snapshots to provide interpolated forcings to the ISM. By comparing temperature forcings from the snapshots, we have evaluated the distance to be roughly 200 to 300 km over which the effects of the ice sheet is small enough (i.e., $<$1°C change). To keep a reasonable computing speed, we have chosen 200 km as the radius of evaluation for the nonlinear method. Let us emphasize here that we acknowledge that temperature is not the only climatic variable modified by an ice sheet and that the latter will alter the climate over farther distances through atmospheric circulation changes. However, because the range of uncertainties in CO_2 reconstructions [*Beerling and Royer*, 2011], Antarctic topography [*Gasson et al*., 2014; *Wilson et al*., 2012], or in the matrix method [*Pollard*, 2010] are limitations to a more precise calibration, we have chosen to limit our study to this simple case.

3. Results

3.1. Constant CO_2 Simulations

The impact of the atmospheric CO_2 concentration on the initiation of a continental scale ice sheet is summarized in Table 2 and in Figures 2 and 4. At 3.5 × PAL, ephemeral ice is present over Antarctica. Only the highest elevations of Antarctica (the Gamburtsev and the Transantarctic Mountains) are periodically covered with very small isolated ice caps during low-insolation times (Figures 2 and 4 and Table 2). Once the climate gets slightly warmer due to orbital parameter variations, the ice melts and vanishes. At 3 × PAL, the glaciation is initiated as soon as the first summer insolation minimum is crossed. Contrary to the simulation at 3.5 × PAL, the ice feedback combined to the lower pCO_2 are strong enough to initiate the continental scale glaciation with only one large ice sheet covering the majority of Antarctica (Figure 4). West Antarctica remains mostly ice free as well as Victoria Land (on the western shores of the modern Ross ice shelf). The total ice volume reaches up to 28×10^6 km^3, 105% of modern Antarctic ice volume ($\approx 27 \times 10^6$ km^3 [*Fretwell et al*., 2013]). At 2.5 × PAL and 2 × PAL, the whole continent is covered with ice (Figure 4), except for a small part of West Antarctica at 2.5 × PAL. For the latter CO_2 concentration, the ice volume is 31×10^6 km^3, while at 2 × PAL, the volume reaches 32.5×10^6 km^3, respectively, 115 and 120% of modern Antarctic ice volume. These values are close to recent modeling estimates [*Wilson et al*., 2013].

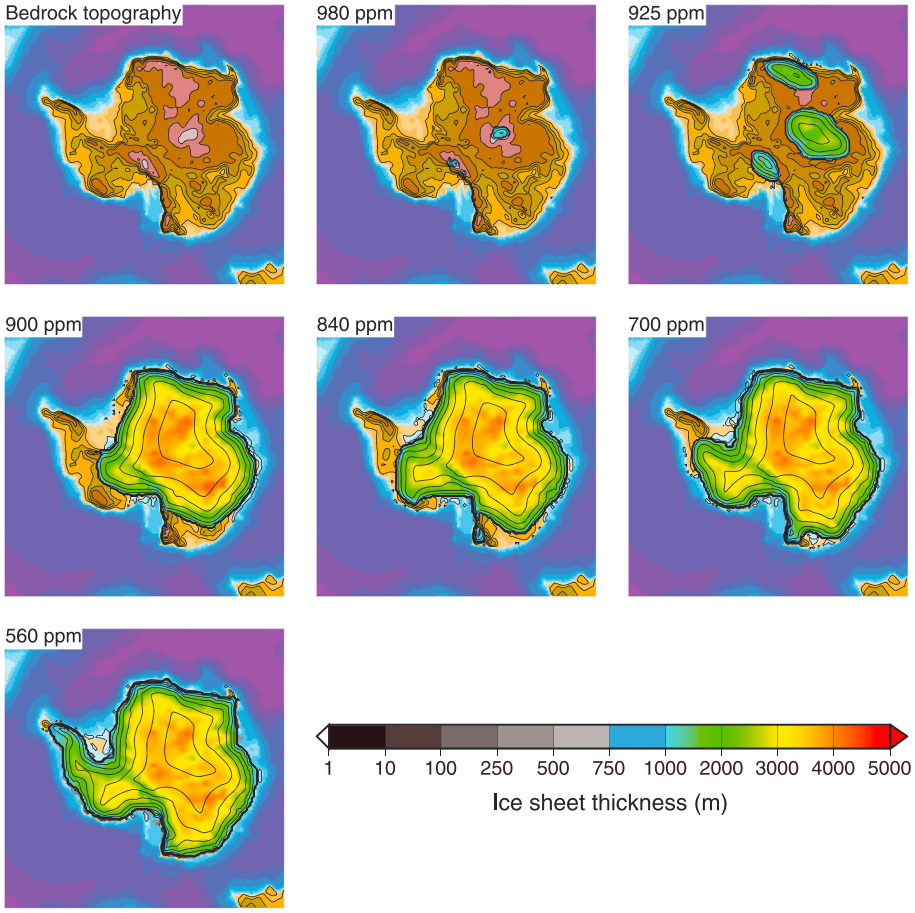

Figure 4. Maximum ice sheet volume attained during the constant CO_2 simulations (see also Figure 2). The corresponding values are given in Table 2.

To refine our estimate of the CO_2 threshold required to initiate a large-scale glaciation, we have carried out two additional simulations with, respectively, 900 and 925 ppm (Figures 2 and 4 and Table 2). At 925 ppm, a very small ice sheet starts to develop following the very strong insolation minimum before 33.9 Ma. It responds dynamically to orbital variations, but as the relatively high CO_2 restricts the ice sheet to high elevations, the amplitude of variations remains low. On the contrary, at 900 ppm, the CO_2 is low enough to produce, via the height-mass balance and ice-albedo feedback, a jump toward a continental scale ice sheet. At first, the snowline only intersects the highest elevations of Antarctica when the summer insolation drops low enough. During the following maximum, the local ice-albedo feedback prevents the melt of the majority of the small ice sheet, which can therefore expand during the following insolation minimum. If at 925 ppm, the CO_2 is always too high for the snowline to cross the high mountain plateaus of Antarctica, at 900 ppm, an insolation minimum enables this threshold to be crossed, which results in a very rapid growth of the ice sheet due to the height-mass balance and ice-albedo feedback [see also, e.g., *Pollard and DeConto*, 2005], leading to a large-scale ice sheet. Once a continental scale is reached, the ice sheet responds dynamically to orbital variations, with larger amplitudes than at 925 ppm because the ice sheet has expanded over large low-elevation areas.

Our new interpolation method results in a modeled CO_2 threshold for large-scale glaciation over Antarctica of approximately 900–925 ppm. This value is significantly higher (≈100–150 ppm) than previous estimates of continental scale glaciation threshold [*DeConto and Pollard*, 2003a] and likely reflects the combined effect of the height-mass balance and the strong ice-albedo feedback; the latter being, for the first time to our knowledge, accounted for such long-term ice sheet variations. The reasons that can be invoked to explain this difference encompass (a) the effects of our coupling method; (b) the sensitivity of climate models,

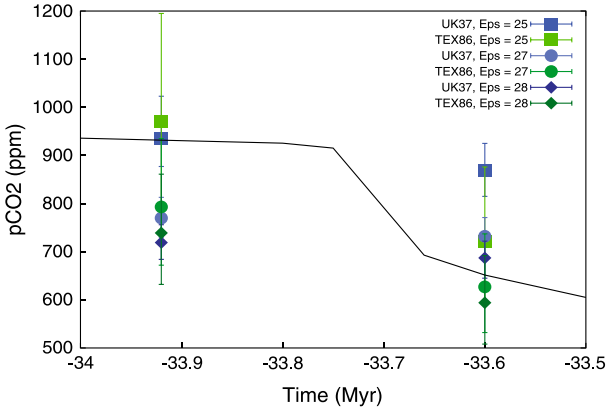

Figure 5. CO_2 data and forcing used in our EOT simulation. Data are from *Pagani et al.* [2011]. Blue-like colors refer to CO_2 derived from alkenones constrained with U^K_{37}′ and green-like colors with TEX_{86}. Estimated pCO_2 concentrations are shown with error bars for different plausible carbon isotope fractionation values (squares: $\varepsilon_f = 25‰$, circles: $\varepsilon_f = 27‰$, and diamonds: $\varepsilon_f = 28‰$).

especially to CO_2; and (c) the differences in the ISM itself, which have been shown to impact the ice sheet growth [*Gasson et al.*, 2014]. This threshold is consistent with the Cenozoic evolution of pCO_2 [*Beerling and Royer*, 2011; *Pagani et al.*, 2005] and intercomparison modeling studies [*Gasson et al.*, 2014]. We also suggest that under lower summer insolation periods than those found between 34 and 33.5 Ma, small to intermediate (10–30 m of equivalent sea level) stable ice sheets could have occurred at CO_2 levels close to or even higher than 1000 ppm. Such low summer insolation occurred many times during the middle Eocene, with values reaching, for instance, 386 W m^{-2} at 41.5 Ma or 394 W m^{-2} at 38.6 Ma, compared to the minimum value of 404 W m^{-2} during the EOT (Figure 2). Hence, even if further work, accounting for a middle Eocene paleogeography, is required to investigate the possible existence of small to intermediate ice sheets during this period [*Dawber and Tripati*, 2011; *Miller et al.*, 2005; *Pekar et al.*, 2005], we can expect that our model will support this case with the combination of approximately 1000 ppm CO_2 concentration and low summer insolation.

3.2. Transient Simulation Over the Eocene-Oligocene Transition

The next step is to extend our interpolation method to use the most recent reconstructions of atmospheric CO_2 variations [*Pagani et al.*, 2011]. Acknowledging the nonnegligible uncertainties associated with these reconstructions, we have chosen to force our model with a decreasing CO_2 function the variations of which are arbitrary, due to the lack of higher-resolution data, but are in agreement with the range of values available (Figure 5). Starting with an initial ice-free Antarctica, an atmospheric CO_2 concentration equal to 925 ppm and the real insolation forcing computed from the study of *Laskar et al.* [2004], we let the ice sheet model run for 500 kyr over the transition. As shown in Figure 6, the model is able to reproduce the two-step transition in a way that is consistent with data both in timing and amplitude. Our simulated ice volume presents a two-step increase separated by a 150–200 kyr plateau. The two steps of the growth simulated by the model are timed at 33.9 and 33.7 Ma and last approximately 50 kyr each. Our ice volume time evolution is well correlated with $\delta^{18}O$ records [*Coxall and Wilson*, 2011; *Coxall et al.*, 2005], the chronology of which is based on the same astronomically calculated variations of the Earth's orbit [*Laskar et al.*, 2004]. Furthermore, data suggest that the first step represents a cooling of about 2–4°C with a small ice volume component, while the second step records a huge ice growth [*Katz et al.*, 2008; *Lear et al.*, 2008; *Pusz et al.*, 2011]. *Scher et al.* [2011] also support this interpretation as they do not record any significant ice-rafted debris (IRD) at Site 738 (Kerguelen Plateau) during the first $\delta^{18}O$ increase (EOT-1), indicating a modest ice sheet. On the contrary, they record an accumulation of IRD peaks during the second excursion (Oi-1), showing that a continental scale ice sheet has developed and reached the ocean. Our simulation presents the same behavior with an increase of roughly 4×10^6 km^3 (≈10 m sea level equivalent considering only the density change between seawater and ice; Table 3) for EOT-1, leading to three small ice sheets located on the high elevations of Antarctica, and a more than 25×10^6 km^3 increase for Oi-1 (≈63 m sea level equivalent; Table 3), completely covering Antarctica with ice. Between these two steps, the ice sheet responds dynamically to orbital changes in agreement with the variability seen in proxy records and previous modeling studies. However, after the major increase, the simulated ice sheet is much less sensitive to orbital variations because of the coupled effect of greatly reduced summer insolation variations and low CO_2 concentrations.

Our matrix method shows the prominent effect of CO_2 and orbital parameters on ice sheet variability. Ice growth always occurs close to a summer insolation minimum during which enough ice has accumulated to

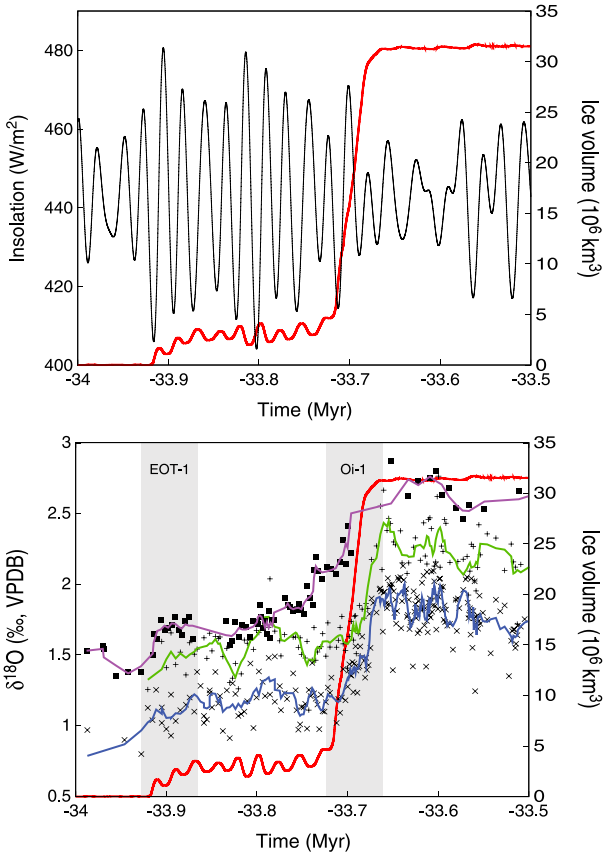

Figure 6. (top) Ice evolution over Antarctica during the EOT compared with insolation variations and (bottom) benthic foraminiferal records. The red curve is the simulated ice growth starting with no ice under a decreasing CO_2 forcing (see Figure 5). Figure 6 (bottom) *Cibicidoides* spp. (tilted crosses) and *O. umbonatus* (straight crosses) records from ODP Site 1218 [*Coxall and Wilson*, 2011] with five-point running means (blue and green curves) and *Cibicidoides* spp. record (black squares) from ODP Site 738 [*Scher et al.*, 2011] with three-point running mean (purple curve). Differences in the absolute values of $\delta^{18}O$ are either due to differences in foraminiferal species or to different drill cores. Note the very well correlated timing between the ice growth periods and the oxygen isotope excursions.

survive the following summer insolation maximum. However, the atmospheric CO_2 concentration remains the main forcing that limits the ice expansion. In Figure 6, the strongest insolation minima are timed at 33.9 Myr and 33.8 Myr; yet only a modest amount of ice accumulates because the CO_2 level is too high. Conversely, a less severe insolation minimum close to 33.7 Myr is sufficient to initiate the major step toward continental ice growth because of the simultaneous decrease in atmospheric CO_2. More generally, the runs with constant CO_2 show that the impact of orbital parameters is really critical for CO_2 levels close to the continental scale glaciation threshold. Above the threshold (925 ppm), the ice sheet responds to orbital variations; however, the higher CO_2 levels dampen its variability because ice is restricted to high elevation areas. When the atmospheric CO_2 concentration decreases (900 ppm run), the amplitude of the ice growth and retreat becomes larger until the crossing of the continental scale glaciation threshold, which results in a rapid, nonlinear growth due to height-mass balance and ice-albedo feedback. When the threshold is crossed (3, 2.5, and 2 × PAL runs), the atmospheric CO_2 concentration is low enough to permit large scale glaciation, and the variability decreases as well because of the cold conditions initiated by the ice sheet feedback. Furthermore, it is interesting to note that in our simulations, the prolonged absence of warm summers is not correlated to major simulated ice growth, as *Coxall et al.* [2005] previously suggested. We find instead that major ice growth is correlated with cold summers followed by warm summers, whereas the absence of cold and warm summers (e.g., 33.65–33.6 Ma) only has a limited impact on ice sheet variability.

Table 3. Ice Increase, Eustatic Sea Level (SL) Drop, and δ_w Increase for an Averaged Isotopic Composition of the Ice of −35‰ or −50‰ Across the EOT[a]

	Ice Increase (10^6 km^3)	Eustatic SL Drop (m)	δ_w Increase (‰) With −35‰ Ice	δ_w Increase (‰) With −50‰ Ice
EOT-1	≈4	≈10	0.10	0.14
Oi-1	≈25	≈63	0.62	0.89

[a]The Eocene ocean area is taken as 365×10^{12} m^2 [*Wilson et al.*, 2013], and the calculation of the $\delta^{18}O_{sw}$ increase is done using the formula

$$\delta_w = \left(\left(\delta^{18}O_{sw} \times V_{totocean}\right) - \left(\delta_{ice} \times V_{totice}\right)\right)/\left(V_{totocean} - V_{totice}\right) - \delta^{18}O_{sw}$$

with the assumption that an ice-free world ocean has a mean $\delta^{18}O_{sw}$ of −1.2‰ and a volume of 1.39×10^9 km^3 [*Shackleton and Kennett*, 1975].

4. Discussion

To provide comparisons with the data and other modeling studies, we estimate the δ_w increase in the ocean associated with each step (Table 3) based on an averaged isotopic composition of glacial ice of either −35 or −50‰, the latter value corresponding to the mean Antarctic ice sheet modern value [*Shackleton and Kennett*, 1975]. Ice sheets in a warmer world may have been less isotopically depleted than modern ones [*DeConto et al*., 2008; *Lear et al*., 2008]; the −35‰ value does consequently account for these potential changes. The isotopic ratio of oxygen within marine organism shells is dependent both on the temperature of waters into which these organisms have calcified and on the ice volume that impacts the mean seawater $\delta^{18}O$. Despite the uncertainties still associated with the disentanglement of these two $\delta^{18}O$ components and those associated with stratigraphic records due to poor constraints on margins, many studies have attempted to give estimates of the $\delta^{18}O_{sw}$ change in the ocean and in sea level variations.

Pekar et al. [2002] derive a 54 ± 10 m for the Oi-1 step while *Houben et al*. [2012] give values of 20 m for EOT-1 and 50–60 m for Oi-1, in agreement with the 75 m estimate of *Pekar and Christie-Blick* [2008]. Other studies give estimates of as much as 25 m for EOT-1 [*Katz et al*., 2008; *Miller et al*., 2009] and 80 ± 25 m for Oi-1 [*Miller et al*., 2009]. *Stocchi et al*. [2013] have simulated an equivalent sea level drop of 69 m for the whole transition using a glacial hydroisostatic adjustment model forced by an Antarctic ISM. A close estimate of 80–90 m is also given by *Wilson et al*. [2013]. Based on $\delta^{18}O$ records from Kerguelen Plateau sites, *Bohaty et al*. [2012] give an estimated early Oligocene ice volume comprised between 15.5 and 33×10^6 km^3 (approximately 42–90 m eustatic sea level) for their most plausible scenario. From their compilation of sites, the average seawater $\delta^{18}O$ increase over the transition reaches 0.6‰ ± 0.15‰. Similarly, from Tanzanian planktonic foraminiferal records, *Lear et al*. [2008] infer a 0.7‰ $\delta^{18}O$ variation associated with EOT-1 among which 0.2‰ is associated with ice volume and the other 0.5‰ with cooling. They estimated the change in seawater $\delta^{18}O$ during the Oi-1 event to reach 0.4‰, yielding a total increase of 0.6‰ over the transition. The latter value is also consistent with the estimates of *Peck et al*. [2010] from Ocean Drilling Program (ODP) Site 1263. *Lear et al*. [2008] also provide ice volume estimations for the EO transition, comprised between 16.9 and 28.4×10^6 km^3 depending on the average isotopic composition of the ice. This is tantamount to a eustatic sea level fall of 46–78 m. *Katz et al*. [2008] record a 0.4‰ seawater $\delta^{18}O$ increase at EOT-1 from three locations—Saint Stephens Quarry (SSQ) in Alabama and ODP Sites 522 and 1218—but no evidence of sea level drop in the SSQ stratigraphic records possibly due to a local hiatus. According to their study, Oi-1 is marked by a 1‰ increase in benthic foraminiferal $\delta^{18}O$ from which up to 0.6‰ would be attributable to the ice volume component. More recently, *Pusz et al*. [2011] recorded a 0.5‰ deep water foraminiferal increase associated with EOT-1 at ODP Sites 1090 and 1265, divided between a 2°C cooling and little if any ice growth (<10 m). They also found a 1‰ benthic $\delta^{18}O$ increase for Oi-1 to which they attributed a 0.75‰ ice volume component (≈70 m eustatic sea level fall).

Mean estimates taking into account all the data presented above yield a total eustatic sea level fall of 40–120 m divided between a 10–30 m fall for EOT-1 and a 40–105 m for Oi-1. The total seawater $\delta^{18}O$ increase is comprised between 0.6 and 1‰, with a larger increase for Oi-1 (0.4–0.75‰) compared to EOT-1 (0.1–0.4‰). Our modeling results reveal an increase in seawater $\delta^{18}O$ comprised between 0.10‰ and 0.14‰ for EOT-1 and 0.62–0.89‰ for Oi-1, depending on the average isotopic composition of the ice (Table 3). This is in good agreement with data from many locations and notably with the recent records of *Pusz et al*. [2011], which are corrected for changes in the carbonate saturation state, the latter being induced by the large-scale drop in the carbonate compensation depth occurring at the EOT [*Coxall et al*., 2005]. These corrected records also produce the closest estimates to our sea level drop results, which give 10 m for EOT-1 and 63 m for Oi-1, yielding a total sea level drop of 70–75 m. Moreover, this amplitude of sea level fall is in quite good agreement with the other records and independent estimates from other Ice Sheet Model simulations [e.g., *Stocchi et al*., 2013], supporting the plausibility of our reconstructed scenario for the Eocene-Oligocene transition.

However, the remaining discrepancies between our modeling results and data records may be explained by a still debated isotopic composition of ancient ice [*DeConto et al*., 2008; *Lear et al*., 2008], uncertainties associated with each proxy, and short-term variations of the atmospheric CO_2 concentration. The latter might indeed be a good candidate to explain these differences, with possible rises and falls affecting the amplitude of the steps. Up to now, however, this hypothesis still lacks evidence, as the latest studies [*Pagani et al*., 2011; *Pearson et al*., 2009] do not resolve pCO_2 variations at less than at least a 100 kyr time scale.

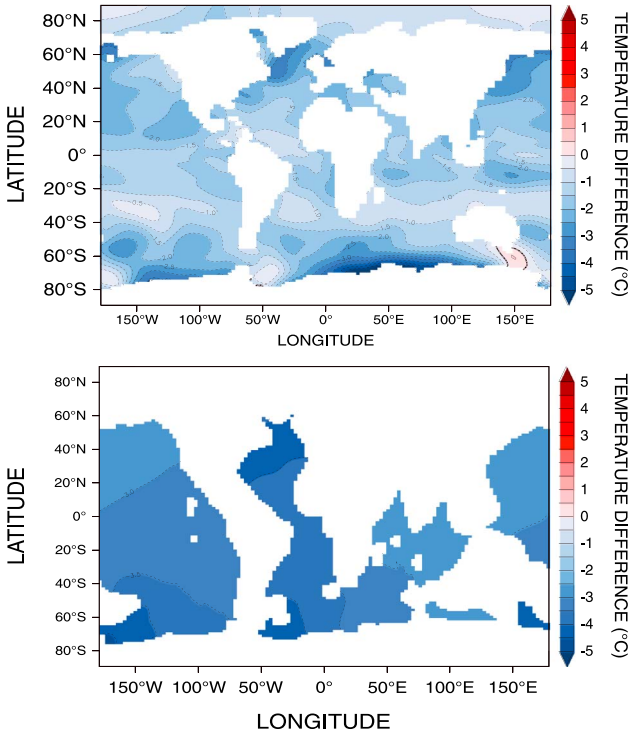

Figure 7. (top) SST (0 to 120 m) and (bottom) deep-sea temperature (2700 to 3500 m) anomalies across the EOT. See also Table 4.

A substantial ocean cooling occurs as well during the EOT. Both surface water and deep ocean recorded cooling of up to several degrees [*Liu et al*., 2009; *Pusz et al*., 2011]. For high-latitude sea surface temperatures, using alkenone unsaturation and tetraether indexes, *Liu et al*. [2009] derive an average 5°C cooling, larger than the Mg/Ca-based reconstructions of *Bohaty et al*. [2012], who report a 2 to 3°C drop in Southern Ocean thermocline waters. Low-latitude sites also reveal a substantial SST cooling, from 2.5°C in Tanzanian planktonic records [*Lear et al*., 2008] to 3 to 6°C in the Gulf of Mexico [*Wade et al*., 2011]. In order to further corroborate our results with the available data, we compare recorded sea surface cooling at several sites with the simulated cooling calculated with our model (Figure 7 and Table 4) for the whole transition. Our results are in rather good agreement for both high- and low-latitude sites. The simulated SST cooling in the Kerguelen Plateau area reaches 2.5°C, which falls exactly within the uncertainties of *Bohaty et al*. [2012]. Off the paleocoast of Tanzania, the cooling attains a slightly smaller 1.5°C compared to the 2.5°C inferred by *Lear et al*. [2008]. However, our simulated cooling is underestimated in both high-latitude southern and northern Atlantic compared to $U^{K}_{37}{}'$ and TEX_{86}-based SST reconstructions [*Liu et al*., 2009]. Our results are nonetheless consistent considering potential uncertainties in paleotemperature proxies. By linearly combining the temperature of the most appropriate snapshots before and after each step, we also tentatively separate the sea surface temperature signal associated with each step to compare with data, providing estimates for both EOT-1 and Oi-1. Results however are largely underestimated, especially for EOT-1 (Table 4).

In the deep ocean, *Katz et al*. [2008] propose a 2.5°C cooling for EOT-1 followed by a 2°C cooling during Oi-1. As shown by *Pusz et al*. [2011], the carbonate saturation state may certainly have affected

Table 4. Multisite Data-Reconstructed Oceanic Cooling for Deep Sea and Surface Waters During the EOT[a]

	Surface Water Cooling (°C)			Deep Sea Cooling (°C)		
	EOT-1	Oi-1	Overall	EOT-1	Oi-1	Overall
Data (model)	2.5[b] (0.2) 3–4[c] (0.5)	<0.5[b] (0.4) 2[c,h]	4–5[d] (2.1) 2.5[b] (1.5) 2–3[e] (2.5)	2–2.5[f] (0.1) 2–2.5[g] (0.2)	1.5[f] (2) 2[g] (2)	3–4[f] (3.9) 4–5[g] (3.8)

[a]The simulated cooling calculated by the model at the same locations as the data is shown into brackets. Please refer to the corresponding papers for exact locations of the data sites. Note that the sum of the simulated cooling during EOT-1 and Oi-1 is not equal to the overall simulated cooling during the transition. Indeed, our overall cooling takes into account the whole prescribed drop in CO_2, whereas calculations for EOT-1 and Oi-1 only include the 50 kyr of each step and thus do only account for roughly half the amplitude of the CO_2 fall.
[b]*Lear et al*. [2008].
[c]*Wade et al*. [2011].
[d]*Liu et al*. [2009].
[e]*Bohaty et al*. [2012].
[f]*Pusz et al*. [2011].
[g]*Katz et al*. [2008].
[h]This value is uncertain due to hiatuses and to the resolution of the TEX_{86} record (see *Wade et al*. [2011]).

deep-sea records, resulting, at Sites 1090 and 1265, in a slightly smaller 2°C and 1.5°C cooling for EOT-1 and Oi-1, respectively. We have also estimated the cooling (both overall and step-by-step) simulated by the model and compared to data (Figure 7 and Table 4). Our simulated deep-sea cooling fits very well with available data when considering the whole E-O transition. We simulate a deep-ocean cooling of approximately 4°C, whereas from South Atlantic [*Katz et al*., 2008; *Pusz et al*., 2011] and Pacific [*Katz et al*., 2008] sites, the data record a 3–5°C drop in deep-sea temperatures. The tentative separation between cooling occurring at EOT-1 and Oi-1 gives, as with SSTs, underestimations of the deep-sea cooling associated with EOT-1 (Table 4).

The causes of the discrepancies between the simulated cooling associated with each step and the recorded cooling reconstructed from data are beyond the scope of this study. The modeling of the exact cooling associated with each step could indeed easily motivate a study of its own. As an example, oceanic current reorganizations are likely to have impacted the temperature of the ocean worldwide, especially in the late Eocene when Antarctica became progressively isolated [e.g., *Stickley et al*., 2004]. However, the changes associated with such current reorganizations are not the focus of the present study, but some studies have investigated this process in the past decade [e.g., *Huber et al*., 2004; *Sijp and England*, 2004; *Sijp et al*., 2011]. Another possibility is a major drop of the atmospheric CO_2 concentration, from levels higher than 1000 ppm to levels close to the glaciation threshold, occurring concomitantly with EOT-1. This large drop could account for the substantial ocean cooling observed in the marine records but is up to now not supported by CO_2 proxies. However, the uncertainties associated with CO_2 proxies [e.g., *Beerling and Royer*, 2011] remain large and mostly unknown, which makes this hypothesis reasonable.

To sum up, our estimates of sea level fall, $\delta^{18}O$ excursions, and both overall deep-sea and sea surface temperature cooling are in good agreement with the available data from various locations across the Earth. As such, this supports our modeling result of the ice sheet volume evolution during the EOT, which is, to date, the only ice sheet modeling reconstruction that reproduces the behavior of the ice sheet at the EOT consistently with data.

5. Conclusion

For the first time, a data-driven (CO_2 and summer insolation) ice sheet model forced by climatic snapshots covering different ice sheet sizes, orbital parameters, and atmospheric CO_2 concentrations is able to simulate the ice evolution through the EOT and to reproduce the timing and the magnitude of the two steps. Simulations under constant atmospheric CO_2 reveal the substantial impact of the combination of the ice feedback (height-mass balance and albedo) and the insolation, which gives a large-scale glaciation threshold of about 900 ppm more than 100–150 ppm higher than previously thought [*DeConto and Pollard*, 2003a]. In agreement with CO_2 reconstructions [*Pagani et al*., 2005], this value also strongly supports the existence of small to intermediate ice sheets during the Eocene. Transient simulations of 500 kyr across the transition reproduce well the two-step ice increase seen in the data [*Coxall and Wilson*, 2011; *Coxall et al*., 2005]. At 33.9 Ma, a favorable low summer insolation cycle initiates the glaciation under a relatively high CO_2 concentration. Because of the latter, only a small ice sheet, restricted to the higher elevations of Antarctica, can develop and respond dynamically to orbital variations. Once a CO_2 threshold is crossed (around 33.7 Ma), the ice sheet responds very rapidly and nonlinearly to the height-mass balance and ice-albedo feedback, which results in a huge increase in the volume of ice over Antarctica. While the atmospheric CO_2 continues to decrease, the ice sheet reaches a full-scale state. The local cooling effect associated with this enormous volume of ice is so strong that further variations in insolation have a completely negligible effect on the ice sheet. Comparisons of our results with $\delta^{18}O$ records using a chronology based on the same orbital reconstructions reveal a very good correlation in terms of age. The estimates of sea level falls and $\delta^{18}O_{sw}$ increases for both steps are also consistent with the data [*Houben et al*., 2012; *Pusz et al*., 2011] as well as the estimates of the cooling during the transition [*Bohaty et al*., 2012; *Pusz et al*., 2011]. Our results highlight the role of orbital parameters in initiating the steps of the transition but show that the main driver remains the concentration in atmospheric CO_2. Carbon dioxide reconstructions at the EOT being up to now still scarce, low resolution, and subject to high uncertainties, there is a real need for more studies to provide better constraints (at time scales of tens of kiloyears) on this crucial component of one of the major climatic changes of the Cenozoic.

Acknowledgments
We are very grateful to Heiko Pälike for his editorial handling and to two anonymous reviewers for their very constructive comments that greatly enhanced the quality of this manuscript. We thank Gilles Ramstein and Pierre Sepulchre for insightful discussions and Helen Coxall and Aimee Pusz for providing some of their data. We thank the CEA/CCRT for providing access to the HPC resources of TGCC under the allocation 2014–012212 made by GENCI. This research was funded by CEA PhD grant CFR and ANR COLORS project.

References

Barrier, E., and B. Vrielynck (2008), *Palaeotectonic Maps of the Middle East*, Commission for the Geologic Map of the World, Paris.
Beerling, D. J., and D. L. Royer (2011), Convergent Cenozoic CO_2 history, *Nat. Geosci.*, *4*(7), 418–420, doi:10.1038/ngeo1186.
Bice, K., E. Barron, and W. Peterson (1998), Reconstruction of realistic Early Eocene paleobathymetry and ocean GCM sensitivity to specified ocean basin configuration, in *Tectonic Boundary Conditions for Climate Reconstructions*, pp. 212–226, Oxford Univ. Press, New York.
Bohaty, S. M., J. C. Zachos, and M. L. Delaney (2012), Foraminiferal Mg/Ca evidence for Southern Ocean cooling across the Eocene-Oligocene transition, *Earth Planet. Sci. Lett.*, *317–318*, 251–261, doi:10.1016/j.epsl.2011.11.037.
Browning, J. V., K. G. Miller, and D. K. Pak (1996), Global implications of lower to middle Eocene sequence boundaries on the New Jersey coastal plain: The icehouse cometh, *Geology*, *24*(7), 639–642.
Coxall, H. K., and P. A. Wilson (2011), Early Oligocene glaciation and productivity in the eastern equatorial Pacific: Insights into global carbon cycling, *Paleoceanography*, *26*, PA2221, doi:10.1029/2010PA002021.
Coxall, H. K., P. A. Wilson, H. Pälike, C. H. Lear, and J. Backman (2005), Rapid stepwise onset of Antarctic glaciation and deeper calcite compensation in the Pacific Ocean, *Nature*, *433*(7021), 53–57, doi:10.1038/nature03185.
Dawber, C. F., and A. K. Tripati (2011), Constraints on glaciation in the middle Eocene (46–37 Ma) from Ocean Drilling Program (ODP) Site 1209 in the tropical Pacific Ocean, *Paleoceanography*, *26*, PA2208, doi:10.1029/2010PA002037.
DeConto, R. M., and D. Pollard (2003a), A coupled climate–ice sheet modeling approach to the Early Cenozoic history of the Antarctic ice sheet, *Palaeogeogr. Palaeoclimatol. Palaeoecol.*, *198*(1–2), 39–52, doi:10.1016/s0031-0182(03)00393-6.
DeConto, R. M., and D. Pollard (2003b), Rapid Cenozoic glaciation of Antarctica induced by declining atmospheric CO_2, *Nature*, *421*, 245–249, doi:10.1038/nature01290.
DeConto, R. M., D. Pollard, P. A. Wilson, H. Pälike, C. H. Lear, and M. Pagani (2008), Thresholds for Cenozoic bipolar glaciation, *Nature*, *455*(7213), 652–656, doi:10.1038/nature07337.
DeConto, R., D. Pollard, and D. Harwood (2007), Sea ice feedback and Cenozoic evolution of Antarctic climate and ice sheets, *Paleoceanography*, *22*, PA3214, doi:10.1029/2006PA001350.
Donnadieu, Y., Y. Goddéris, and N. Bouttes (2009), Exploring the climatic impact of the continental vegetation on the Mezosoic atmospheric CO_2 and climate history, *Clim. Past*, *5*, 85–96, doi:10.5194/cp-5-85-2009.
Fretwell, P., H. D. Pritchard, D. G. Vaughan, J. Bamber, N. Barrand, R. Bell, C. Bianchi, R. Bingham, D. Blankenship, and G. Casassa (2013), Bedmap2: Improved ice bed, surface and thickness datasets for Antarctica, *Cryosphere*, *7*(1), 375–393, doi:10.5194/tc-7-375-2013.
Gasson, E., et al. (2014), Uncertainties in the modelled CO_2 threshold for Antarctic glaciation, *Clim. Past*, *10*(2), 451–466, doi:10.5194/cp-10-451-2014.
Herrington, A. R., and C. J. Poulsen (2011), Terminating the last interglacial: The role of ice sheet-climate feedbacks in a GCM asynchronously coupled to an ice sheet model, *J. Clim.*, *25*(6), 1871–1882, doi:10.1175/jcli-d-11-00218.1.
Horton, D. E., and C. J. Poulsen (2009), Paradox of late Paleozoic glacioeustasy, *Geology*, *37*(8), 715–718, doi:10.1130/g30016a.1.
Houben, A. J. P., C. A. van Mourik, A. Montanari, R. Coccioni, and H. Brinkhuis (2012), The Eocene-Oligocene transition: Changes in sea level, temperature or both?, *Palaeogeogr. Palaeoclimatol. Palaeoecol.*, *335–336*, 75–83, doi:10.1016/j.palaeo.2011.04.008.
Hourdin, F., I. Musat, S. Bony, P. Braconnot, F. Codron, J.-L. Dufresne, L. Fairhead, M.-A. Filiberti, P. Friedlingstein, and J.-Y. Grandpeix (2006), The LMDZ4 general circulation model: Climate performance and sensitivity to parametrized physics with emphasis on tropical convection, *Clim. Dyn.*, *27*(7–8), 787–813, doi:10.1007/s00382-006-0158-0.
Huber, M., H. Brinkhuis, C. E. Stickley, K. Döös, A. Sluijs, J. Warnaar, S. A. Schellenberg, and G. L. Williams (2004), Eocene circulation of the Southern Ocean: Was Antarctica kept warm by subtropical waters?, *Paleoceanography*, *19*, PA4026, doi:10.1029/2004PA001014.
Iturralde-Vinent, M. A., and R. D. E. MacPhee (1999), Paleogeography of the Caribbean region: Implications for cenozoic biogeography, *Bull. Am. Mus. Nat. Hist.*, *238*, 1–95.
Jacob, R. (1997), *Low Frequency Variability in a Simulated Atmosphere Ocean System*, Univ. of Wisconsin-Madison, Madison, Wis.
Katz, M. E., K. G. Miller, J. D. Wright, B. S. Wade, J. V. Browning, B. S. Cramer, and Y. Rosenthal (2008), Stepwise transition from the Eocene greenhouse to the Oligocene icehouse, *Nat. Geosci.*, *1*(5), 329–334, doi:10.1038/ngeo179.
Kennett, J. P. (1977), Cenozoic evolution of Antarctic glaciation, the circum-Antarctic Ocean, and their impact on global paleoceanography, *J. Geophys. Res.*, *82*(27), 3843–3860, doi:10.1029/JC082i027p03843.
Kennett, J. P., and N. F. Exon (2004), Paleoceanographic evolution of the Tasmanian Seaway and its climatic implications, *Geophys. Monogr. Ser.*, *151*, 345–367, doi:10.1029/151GM19.
Laskar, J., P. Robutel, F. Joutel, M. Gastineau, A. C. M. Correia, and B. Levrard (2004), A long term numerical solution for the insolation quantities of the Earth, *Astron. Astrophys.*, *428*, 261–185.
Lear, C. H., T. R. Bailey, P. N. Pearson, H. K. Coxall, and Y. Rosenthal (2008), Cooling and ice growth across the Eocene-Oligocene transition, *Geology*, *36*(3), 251–254, doi:10.1130/g24584a.1.
Lefebvre, V., Y. Donnadieu, P. Sepulchre, D. Swingedouw, and Z.-S. Zhang (2012), Deciphering the role of southern gateways and carbon dioxide on the onset of the Antarctic Circumpolar Current, *Paleoceanography*, *27*, PA4201, doi:10.1029/2012PA002345.
Liu, Z., M. Pagani, D. Zinniker, R. DeConto, M. Huber, H. Brinkhuis, S. R. Shah, R. M. Leckie, and A. Pearson (2009), Global cooling during the Eocene-Oligocene climate transition, *Science*, *323*, 1187–1190, doi:10.1126/science.1166368.
Miller, K. G., J. D. Wright, and J. V. Browning (2005), Visions of ice sheets in a greenhouse world, *Mar. Geol.*, *217*(3–4), 215–231, doi:10.1016/j.margeo.2005.02.007.
Miller, K. G., J. D. Wright, M. E. Katz, B. S. Wade, J. V. Browning, B. S. Cramer, and Y. Rosenthal (2009), Climate threshold at the Eocene-Oligocene transition: Antarctic ice sheet influence on ocean circulation, *Geol. Soc. Am. Spec. Pap.*, *452*, 169–178, doi:10.1130/2009.2452(11).
Pagani, M., J. Zachos, K. H. Freeman, B. Tipple, and S. Bohaty (2005), Marked decline in atmospheric carbon dioxide concentrations during the Paleogene, *Science*, *309*(5734), 600–603, doi:10.1126/science.1110063.
Pagani, M., M. Huber, Z. Liu, S. M. Bohaty, J. Henderiks, W. Sijp, S. Krishnan, and R. M. DeConto (2011), The role of carbon dioxide during the onset of Antarctic glaciation, *Science*, *334*(6060), 1261–1264, doi:10.1126/science.1203909.
Pearson, P. N., G. L. Foster, and B. S. Wade (2009), Atmospheric carbon dioxide through the Eocene-Oligocene climate transition, *Nature*, *461*(7267), 1110–1113, doi:10.1038/nature08447.
Peck, V. L., J. Yu, S. Kender, and C. R. Riesselman (2010), Shifting ocean carbonate chemistry during the Eocene-Oligocene climate transition: Implications for deep-ocean Mg/Ca paleothermometry, *Paleoceanography*, *25*, PA4219, doi:10.1029/2009PA001906.
Pekar, S. F., and N. Christie-Blick (2008), Resolving apparent conflicts between oceanographic and Antarctic climate records and evidence for a decrease in pCO_2 during the Oligocene through early Miocene (34–16 Ma), *Palaeogeogr. Palaeoclimatol. Palaeoecol.*, *260*(1–2), 41–49, doi:10.1016/j.palaeo.2007.08.019.

Pekar, S. F., N. Christie-Blick, M. A. Kominz, and K. G. Miller (2002), Calibration between eustatic estimates from backstripping and oxygen isotopic records for the Oligocene, *Geology*, *30*(10), 903–906, doi:10.1130/0091-7613.

Pekar, S. F., A. Hucks, M. Fuller, and S. Li (2005), Glacioeustatic changes in the early and middle Eocene (51–42 Ma): Shallow-water stratigraphy from ODP Leg 189 Site 1171 (South Tasman Rise) and deep-sea $\delta^{18}O$ records, *Geol. Soc. Am. Bull.*, *117*(7–8), 1081–1093, doi:10.1130/b25486.1.

Pollard, D. (2010), A retrospective look at coupled ice sheet–climate modeling, *Clim. Change*, *100*(1), 173–194, doi:10.1007/s10584-010-9830-9.

Pollard, D., and R. M. DeConto (2005), Hysteresis in Cenozoic Antarctic ice-sheet variations, *Global Planet. Change*, *45*(1–3), 9–21, doi:10.1016/j.gloplacha.2004.09.011.

Poulsen, C., and R. Jacob (2004), Factors that inhibit snowball Earth simulation, *Paleoceanography*, *19*, PA4021, doi:10.1029/2004PA001056.

Pusz, A. E., R. C. Thunell, and K. G. Miller (2011), Deep water temperature, carbonate ion, and ice volume changes across the Eocene-Oligocene climate transition, *Paleoceanography*, *26*, PA2205, doi:10.1029/2010PA001950.

Ritz, C., V. Rommelaere, and C. Dumas (2001), Modeling the evolution of Antarctic ice sheet over the last 420,000 years: Implications for altitude changes in the Vostok region, *J. Geophys. Res.*, *106*(D23), 31,943–31,964, doi:10.1029/2001JD900232.

Scher, H. D., S. M. Bohaty, J. C. Zachos, and M. L. Delaney (2011), Two-stepping into the icehouse: East Antarctic weathering during progressive ice-sheet expansion at the Eocene-Oligocene transition, *Geology*, *39*(4), 383–386, doi:10.1130/g31726.1.

Scotese, C. (2001), *Digital Paleogeographic Map Archive on CD-ROM*, PALEOMAP Project, Arlington, Tex.

Shackleton, N., and J. Kennett (1975), Paleotemperature history of the Cenozoic and the initiation of Antarctic glaciation: Oxygen and carbon isotope analyses in DSDP Sites 277, 279, and 281, *Initial Rep. Deep Sea Drill. Proj.*, *29*, 743–755.

Sijp, W. P., and M. H. England (2004), Effect of the Drake Passage throughflow on global climate, *J. Phys. Oceanogr.*, *34*(5), 1254–1266, doi:10.1175/1520-0485(2004)034.

Sijp, W. P., M. H. England, and M. Huber (2011), Effect of the deepening of the Tasman Gateway on the global ocean, *Paleoceanography*, *26*, PA4207, doi:10.1029/2011PA002143.

Stickley, C. E., H. Brinkhuis, S. A. Schellenberg, A. Sluijs, U. Röhl, M. Fuller, M. Grauert, M. Huber, J. Warnaar, and G. L. Williams (2004), Timing and nature of the deepening of the Tasmanian Gateway, *Paleoceanography*, *19*, PA4027, doi:10.1029/2004PA001022.

Stocchi, P., et al. (2013), Relative sea-level rise around East Antarctica during Oligocene glaciation, *Nat. Geosci.*, *6*, 380–384, doi:10.1038/ngeo1783.

Tigchelaar, M., A. von der Heydt, and H. Dijkstra (2011), A new mechanism for the two-step $d^{18}O$ signal at the Eocene-Oligocene boundary, *Clim. Past*, *7*, 235–247, doi:10.5194/cp-7-235-2011.

Tripati, A., J. Backman, H. Elderfield, and P. Ferretti (2005), Eocene bipolar glaciation associated with global carbon cycle changes, *Nature*, *436*(7049), 341–346, doi:10.1038/nature03874.

Wade, B. S., A. J. P. Houben, W. Quaijtaal, S. Schouten, Y. Rosenthal, K. G. Miller, M. E. Katz, J. D. Wright, and H. Brinkhuis (2011), Multiproxy record of abrupt sea-surface cooling across the Eocene-Oligocene transition in the Gulf of Mexico, *Geology*, *40*(2), 159–162, doi:10.1130/g32577.1.

Wilson, D. S., S. S. R. Jamieson, P. J. Barrett, G. Leitchenkov, K. Gohl, and R. D. Larter (2012), Antarctic topography at the Eocene-Oligocene boundary, *Palaeogeogr. Palaeoclimatol. Palaeoecol.*, *335–336*, 24–34, doi:10.1016/j.palaeo.2011.05.028.

Wilson, D. S., D. Pollard, R. M. DeConto, S. S. Jamieson, and B. P. Luyendyk (2013), Initiation of the West Antarctic Ice Sheet and estimates of total Antarctic ice volume in the earliest Oligocene, *Geophys. Res. Lett.*, *40*, 4305–4309, doi:10.1002/grl.50797.

Zachos, J., M. Pagani, L. Sloan, E. Thomas, and K. Billups (2001), Trends, rhythms, and aberrations in global climate 65 Ma to present, *Science*, *292*(5517), 686–693, doi:10.1126/science.1059412.